Holocene climate variability in the western Mediterranean region from a deepwater sediment record

J. Frigola,[1] A. Moreno,[2] I. Cacho,[1] M. Canals,[1] F. J. Sierro,[3] J. A. Flores,[3] J. O. Grimalt,[4] D. A. Hodell,[5] and J. H. Curtis[5]

Received 21 April 2006; revised 3 December 2006; accepted 3 December 2006; published 4 May 2007.

[1] The detailed analysis of the International Marine Past Global Changes Study core MD99-2343 recovered from a sediment drift at 2391 m water depth north of the island of Minorca illustrates the effects of climate variability on thermohaline circulation in the western Mediterranean during the last 12 kyr. Geochemical ratios associated with terrigenous input resulted in the identification of four phases representing different climatic and deepwater overturning conditions in the Western Mediterranean Basin during the Holocene. Superimposed on the general trend, eight centennial- to millennial-scale abrupt events appear consistently in both grain size and geochemical records, which supports the occurrence of episodes of deepwater overturning reinforcement in the Western Mediterranean Basin. The observed periodicity for these abrupt events is in agreement with the previously defined Holocene cooling events of the North Atlantic region, thus supporting a strong Atlantic-Mediterranean climatic link at high-frequency time intervals during the last 12 kyr. The rapid response of the Mediterranean thermohaline circulation to climate change in the North Atlantic stresses the importance of atmospheric teleconnections in transferring climate variability from high latitudes to midlatitudes.

Citation: Frigola, J., A. Moreno, I. Cacho, M. Canals, F. J. Sierro, J. A. Flores, J. O. Grimalt, D. A. Hodell, and J. H. Curtis (2007), Holocene climate variability in the western Mediterranean region from a deepwater sediment record, *Paleoceanography*, *22*, PA2209, doi:10.1029/2006PA001307.

1. Introduction

[2] The Holocene (last ~10 kyr) has been classically considered a climatically stable episode, especially when compared with climate changes of the last glacial period. However, there is increasing evidence of significant climate variability at orbital and suborbital scales during the present interglacial [*Bianchi and McCave*, 1999; *Bond et al.*, 2001; *Magny et al.*, 2002; *Kuhlmann et al.*, 2004; *Mayewski et al.*, 2004; *Alley and Agustsdottir*, 2005].

[3] Orbitally induced differences in seasonal insolation have determined the long-term climatic evolution of the Holocene with a warm Climate Optimum during the early-to-mid Holocene and a transition to colder conditions around 5 ka [*COHMAP Members*, 1988; *Cheddadi et al.*, 1997, 1998; *Prentice et al.*, 1998; *Claussen et al.*, 1999; *Magny et al.*, 2002; *Davis et al.*, 2003; *Sbaffi et al.*, 2004]. Superimposed on this pattern are events of rapid climate change with periods of 2800–2000, 1500 and 900 years [*Mayewski et al.*, 2004]. While solar flux variability has been proposed to be the main forcing of these Holocene events [*O'Brien et al.*, 1995; *Bond et al.*, 2001; *Rohling et al.*, 2002; *Mayewski et al.*, 2004], oscillations in the production rates of the North Atlantic Deep Water (NADW) and in the poleward heat transport could also have triggered or amplified such instabilities [*Bond et al.*, 1997; *Bianchi and McCave*, 1999; *Schulz and Paul*, 2002; *Oppo et al.*, 2003]. In any case, the direct causative mechanism remains unknown.

[4] Paleoclimatic records have demonstrated the high sensitivity of the western Mediterranean region to rapid climate changes during the last glacial interval, including Dansgaard/Oeschger and Heinrich events, thereby supporting the view of a strong link between the Mediterranean and the North Atlantic climate [*Rohling et al.*, 1998, 2002; *Cacho et al.*, 1999, 2000, 2001; *Moreno et al.*, 2002, 2004; *Martrat et al.*, 2004; *Sierro et al.*, 2005]. This rapid connection between both regions has been interpreted to result from the entrance of cold surface waters into the Mediterranean Sea through the Strait of Gibraltar, but also from the intensification of the atmospheric circulation. A strengthened westerly system enhanced the marine overturning cell in the Gulf of Lion leading to a more efficient formation of Western Mediterranean Deep Water (WMDW) and to the enhancement of deep circulation [*Cacho et al.*, 2001; *Sierro et al.*, 2005].

[5] In contrast to the glacial period, information about Holocene rapid variability in the western Mediterranean region and its links to North Atlantic climate is comparatively scarce. One of the most useful proxies for the study of

[1]Consolidated Research Group Marine Geosciences, Department of Stratigraphy, Paleontology and Marine Geosciences, Faculty of Geology, University of Barcelona, Barcelona, Spain.
[2]Pyrenean Institute of Ecology, Spanish Research Scientific Council, Zaragoza, Spain.
[3]Department of Geology, University of Salamanca, Salamanca, Spain.
[4]Department of Environmental Chemistry, Institute of Chemical and Environmental Research-Spanish Research Scientific Council, Barcelona, Spain.
[5]Department of Geological Sciences, University of Florida, Gainesville, Florida, USA.

0883-8305/07/2006PA001307

WMDW formation and circulation during glacial periods, carbon and oxygen isotopic records from *Cibicidoides spp* foraminifera, is lacking during the Holocene because of poor ventilation and oxygenation conditions of deep waters that caused the disappearance of this species [*Caralp*, 1988; *Reguera*, 2004]. Core MD99-2343 was recovered from the deepwater Minorca sediment drift in the path of the southward branch of the WMDW. In this study, we use grain size distributions and bulk geochemical ratios of terrigenous material down this core to reconstruct Holocene changes in WMDW.

2. Study Area

2.1. Climate and Physical Oceanography Setting

[6] The climate regime of the Mediterranean region is transitional between the temperate maritime type and the arid subtropical desert climate [*Barry and Chorley*, 1998]. The Icelandic low–Azores high system controls present-day meteorology and climate in western Europe including the western Mediterranean region. Summers in the western Mediterranean are usually hot and dry because of the influence of the expanded Azores anticyclone. The southward displacement of the anticyclone during winter allows Atlantic depressions to enter the western Mediterranean region bringing high atmospheric instability and wetter conditions. At decadal scale, this pattern is known as the North Atlantic Oscillation (NAO), which modulates much of the present-day climate variability in this region [*Rodó et al.*, 1997]. The NAO system and the strong influence of the Mediterranean Sea expose the region to large-scale climate changes [*Bolle*, 2003]. The western Mediterranean region is also influenced by Saharan air masses that transport considerable amounts of dust toward the Mediterranean Sea and farther north [*Prospero*, 1996]. This short overview highlights the complexity of the climatic behavior of the western Mediterranean region and evidences its high sensitivity to heat and moisture flux variations.

[7] Because of winter southward displacement of the Azores high, Atlantic depressions follow southern trajectories coming into the Mediterranean region more frequently [*Barry and Chorley*, 1998]. This process leads to the formation of strong and cold northerly and northwesterly winds in the Rhône and Ebro valleys funneling the airflow into the western Mediterranean (i.e., Mistral and Cierzo winds, respectively). These winds cause strong evaporation and cooling offshore in the Gulf of Lion thus increasing surface water density until it sinks to greater depths [*MEDOC*, 1970; *Lacombe et al.*, 1985; *Millot*, 1999]. This process gives birth to the formation of the Western Mediterranean Deep Water (WMDW), which fills the deepest part of the Western Mediterranean Basin (Figure 1). Deep water formation in the Gulf of Lion depends on wind stress variability but is also affected by the amount and depth of the Levantine Intermediate Water (LIW) before WMDW formation events [*Pinardi and Masetti*, 2000]. As consequence of the negative balance of water created by the excess of evaporation over fresh water input in the Mediterranean Sea a compensating surface Atlantic water layer enters through the Strait of Gibraltar as Modified Atlantic Water (MAW) (Figure 1) [*Millot*, 1999]. The dense LIW and WMDW leave the Mediterranean Basin through the Strait of Gibraltar forming the deep Mediterranean Outflow Water (MOW) [*Millot*, 1999].

[8] In the northwestern Mediterranean Sea the Balearic Promontory influences the circulation acting as a topographic barrier. The dense WMDW that forms and sinks in the Gulf of Lion flows south and southwestward into the Valencia Trough at depths closer to 2000 m [*Millot*, 1999] (Figure 1). When the deep current encounters the Balearic Promontory it shifts direction eastward and southeastward bordering the Minorca base of slope. The abruptness of the Balearic slope and the topographically induced change in the current direction likely result in an intensification of the current, as this process has been described for the North Atlantic deep sediment drifts [*McCave and Tucholke*, 1986]. Off Minorca this has led to the formation of the Minorca peripheral depression and associated sediment drift [*Velasco et al.*, 1996] (Figure 2a) where our core MD99-2343 was recovered.

2.2. Particle Sources and Sedimentary Setting

[9] Sediment is supplied to the northwestern Mediterranean Sea mainly by fluvial discharge from the north, by aeolian inputs form the south, and by primary production from surface waters. The two main rivers are the Rhône and the Ebro (Figure 1) with estimated historical pre-damming sediment fluxes of 30×10^6 t yr^{-1} and $17–25 \times 10^6$ t yr^{-1}, respectively [*United Nations Environment Programme*, 2003]. However, only 10% of the fluvial discharge reaches the deep basin while the remaining 90% is deposited in deltaic and inner continental shelf areas [*Martin et al.*, 1989]. Saharan dust fluxes account for 10–20% of present-day deep-sea sedimentation in the western Mediterranean [*Loyë-Pilot et al.*, 1986; *Zuo et al.*, 1991; *Guerzoni et al.*, 1997] although this contribution may have changed substantially through time [*Moreno et al.*, 2002; *Weldeab et al.*, 2003]. The contribution of local pelagic, mostly carbonate particles is limited by the oligotrophic character of most of the western Mediterranean Sea [*Bethoux et al.*, 1998]. In any case, at the location of the studied sediment core, carbonate may also have been contributed by shelf edge spillover processes from the nearby Balearic Promontory [*Maldonado and Stanley*, 1979; *Maldonado and Canals*, 1982].

[10] High-resolution seismic reflection profiles across the Minorca drift show a reflector configuration that is typical of contourite drifts (Figure 2b) [*Vanney and Mougenot*, 1981; *Stow*, 1982; *Stow et al.*, 2002]. While the peripheral depression is filled with coarse sediment [*Canals*, 1980] it is assumed that the fine fraction escaped out of the depression and contributed to the development of the sediment drift in its way toward the basin centre. The MD99-2343 site on the Minorca drift, and the drift itself, occupy a relatively shallower position [*Alonso et al.*, 1995] that is beyond the direct influence of turbidite sedimentation (Figure 2a). However, it is likely that suspended particles escaping from the turbidite systems to the west (Ebro margin) and north (Gulf of Lion margin) may have been caught by the near-bottom circulation and added to the background sedimen-

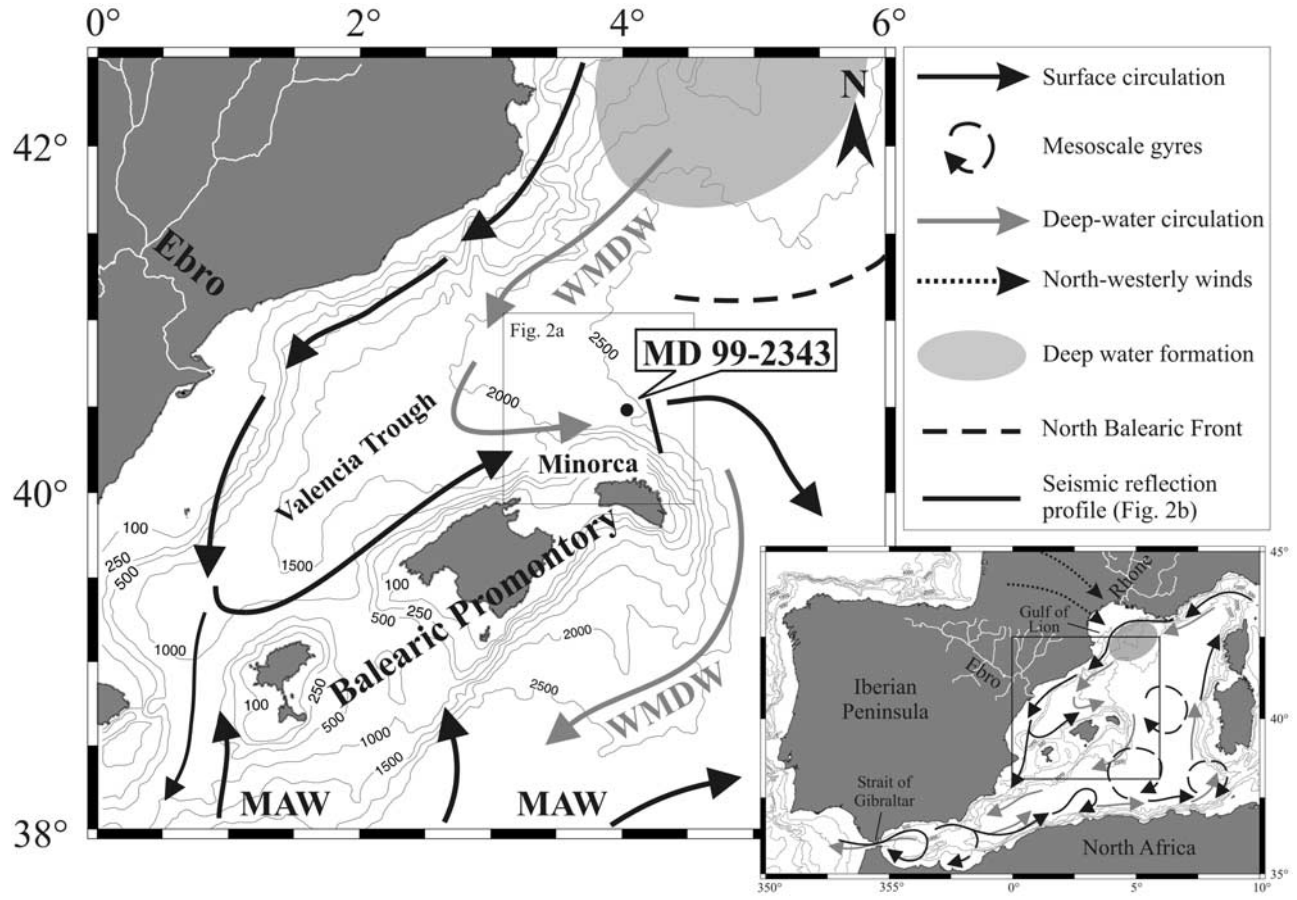

Figure 1. Bathymetric map of the study area showing the general surface and deepwater circulation patterns and the position of core MD99-2343. The box in the main map shows the location of Figure 2a, while the solid line illustrates the location of the seismic reflection profile in Figure 2b. WMDW is Western Mediterranean Deep Water; MAW is Modified Atlantic Water.

tation of the Minorca drift (Figure 2a). Large-scale bed forms found in the deep northwestern Mediterranean Basin further indicate that bottom currents likely played a significant role in the shaping of the seafloor, and thus in sediment particle transport, winnowing and sorting in the recent past [*Mauffret et al.*, 1982; *Maldonado et al.*, 1985; *Palanques et al.*, 1995; *Acosta*, 2005]. Although no current meter data exist for the vicinity of the core site, near-bottom current measurements during a 3-month period at 1800 m water depth in the Gulf of Lion deep margin, where WMDW formation takes place, gave maximum values of 50 cm s^{-1} and mean values of 20 cm s^{-1} [*Millot and Monaco*, 1984].

3. Material and Methods

[11] Sediment core MD99-2343 was recovered with a Calypso piston corer north of Minorca at 40°29.84′N, 04°01.69′E and 2391 m of water depth in the northwestern Mediterranean Sea (Figure 1), during Leg 5 of the R/V Marion Dufresne expedition within the International Marine Past Global Changes Study (IMAGES) programme. From the total 32.44 m of core length, only the top 4 m corresponding to the last 12 kyr are discussed in this paper. The top 4 m consists of grey nannofossil and foraminifer silty clay. Layers with high content of pteropod and gastropod shell fragments have been also observed all along the upper core section. As a general rule, one centimeter thick sediment samples were taken every 4 to 6 cm for oxygen and carbon isotope analyses of foraminifer shells, and grain size and major element composition analyses of the bulk sediment. Additional samples for grain size analyses were collected at 2 cm resolution over selected intervals.

[12] Samples for isotope analyses were washed over a 63-μm sieve and the retained fraction was dried and dry-sieved again using a 150-μm sieve. About 10 mg of *Globorotalia inflata* and *Globigerina bulloides* were hand-picked for radiocarbon isotope analyses. The AMS ^{14}C analyses were performed in the U.S. National Ocean Sciences Accelerator Mass Spectrometry Facility (NOSAMS). The ages were calibrated with the standard marine correction of 408 years and the regional average marine reservoir correction (ΔR) for the western Mediterranean Sea by means of the Calib 5.0.1 programme [*Stuiver and Reimer*, 1993] and the MARINE04 calibration curve [*Hughen et al.*, 2004].

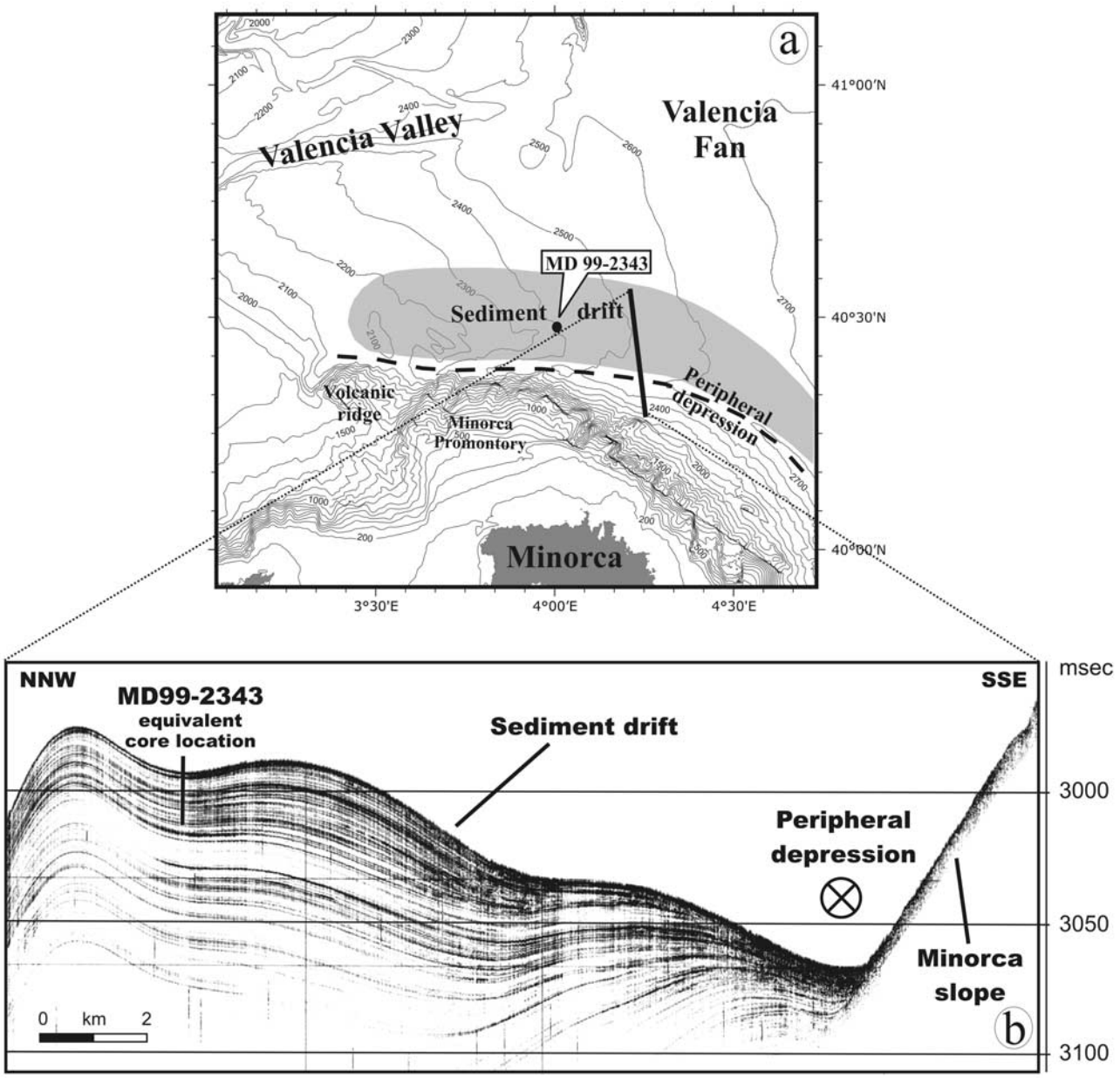

Figure 2. (a) Detailed bathymetric map showing the main seafloor features nearby core MD99-2343. Shaded area roughly delimits the Minorca sediment drift. The abrupt step on the NE Minorca slope is the result from the merging of the high-resolution swath bathymetry data set with the General Bathymetric Chart of the Oceans (GEBCO) digital database [*Intergovernmental Oceanographic Commission et al.*, 2003]. (b) Very high resolution seismic reflection profile across the Minorca sediment drift and peripheral depression (modified from *Velasco et al.* [1996]). The cross within a circle represents the direction of the contour current that is normal to the image. Equivalent position of core MD99-2343 is also shown.

[13] Approximately 5 to 10 specimens of *Globigerina bulloides* from the 300–350 μm size fraction were picked to measure stable isotope ratios. Foraminifer tests were soaked in 15% H_2O_2 to remove organic matter and sonically cleaned in methanol to remove fine-grained particles. The foraminifer calcite was loaded into individual reaction vessels and each sample was reacted with 3 drops of H_3PO_4 (specific gravity = 1.92) using a Finnigan MAT Kiel III carbonate preparation device. Isotope ratios were measured online using a Finnigan MAT 252 mass spectrometer. Analytical precision was estimated to be ±0.08‰ for $\delta^{18}O$ and ±0.03‰ for $\delta^{13}C$ (1σ) by measuring 8 standards (NBS-19) with each carousel containing 38 samples. All isotope results are reported in standard delta notation relative to V-PDB [*Coplen*, 1996].

Table 1. Age Model for Core MD99-2343[a]

Isotope Event or Radiocarbon Sample/Foram Type	Depth, cm	^{14}C Age, years	Calendar Years
AMS ^{14}C/multispecific	28	790 (±40)	386 ± 55
AMS ^{14}C/*G. inflata*[b]	88	3,110 (±30)	2,816 ± 50
AMS ^{14}C/multispecific	118	3,390 (±50)	3,225 ± 80
AMS ^{14}C/*G. inflata*[b]	208	5,720 (±40)	6,091 ± 70
AMS ^{14}C/multispecific	238	6,210 (±50)	6,601 ± 70
AMS ^{14}C/*G. inflata*[b]	308	7,700 (±40)	8,110 ± 60
T1b, onset of the Holocene	354		10,696[c]
AMS ^{14}C/*G. bulloides*[b]	398	10,650 (±50)	11,883 ± 230
AMS ^{14}C/*G. inflata*[b]	418	11,200 (±50)	12,811 ± 30
AMS ^{14}C/*G. bulloides*[b]	568	13,850 (±40)	15,912 ± 190
AMS ^{14}C/multispecific	604	14,550 (±110)	16,822 ± 240

[a]New and previous ^{14}C AMS dates after *Sierro et al.* [2005] calibrated with the Calib 5.0.1 programme [*Stuiver and Reimer*, 1993]. Linear interpolation between dated points was performed with the AnalySeries Version 1.1 [*Paillard et al.*, 1996].

[b]New ^{14}C AMS dates.

[c]Tie point used for the age model of core MD99-2343 by correlation with the oxygen isotopic record from core MD95-2043 in the near Alboran Sea.

[14] Grain size was measured on the total fraction and the noncarbonate fraction after removing organic matter and carbonates by treatment with excess H_2O_2 and HCl, respectively. A Coulter LS 100 Laser Particle Size Analyser (CLS), which determines particle grain sizes between 0.4 and 900 μm, was used to determine grain size distributions as volume percentages. The laser diffraction size analyzer principle is based on the measurement of the diffraction angle produced by the particles when a laser beam goes through the sample in an aqueous solution. The correlation between diffraction angle and particle size is opposite [*McCave et al.*, 1986]. Since diffraction is assumed to be given by spherical particles, the resulting particle size is that diameter (known as equivalent spherical diameter). Subsequently, laser diffraction methods are claimed to underestimate plate-shaped clay mineral percentages. To correct such effect we have followed the method proposed by *Konert and Vandenberghe* [1997]. CLS precision and accuracy is tested by systematic control runs using latex microspheres with predefined diameters. The high precision (reproducibility) of the measurements was demonstrated by small variations in the mean diameter (0.97% of variation) and in the standard deviation (1.37% of variation). The accuracy of the measurements, as indicated by the relative departure from the nominal mean diameter is 0.30%, corresponding to absolute deviations between 0.09 and 0.34 μm. Additional test runs were performed using microsphere assemblages with mixed grain sizes to ensure that CLS accurately determined polymodal grain size distributions.

[15] We discuss grain size results as the median of each sample since it represents the distribution midpoint and it usually constitutes a more representative value of the grain size distribution than the mean. In order to extract palaeoclimate information from a mixture of sediments with different sources numerical-statistical modeling of large grain size data sets provides the best results [*Weltje and Prins*, 2003]. However, core MD99-2343 was recovered on a contouritic drift built by the influence of near bottom currents where minor or no changes in sediment sources are expected (see below). Subsequently, instead of statistical modeling of end-members, we have considered the UP10 fraction, which composes the volume percentage of the fraction coarser than 10 μm, a good indicator of deep currents variability at this site. The UP10 integrates the sortable silt fraction (SS, 10–63 μm), defined as the coarser fraction of the silt with noncohesive behavior during transport and deposition [*McCave et al.*, 1995], while taking also into account the influence of the fine sand subpopulation (>63 μm) that could be reworked by strong contour currents. Finally, the silt/clay ratio has also proven to be useful for the study of deepwater currents intensity [*Hall and McCave*, 2000].

[16] The percentages of major elements in sediment samples were determined by means of X-ray fluorescence using a Philips PW 2400 sequential wavelength X-ray spectrometer. Prior to the analyses, samples were dried at 100°C, and then ground and homogenized in an agate mortar. 0.3 g of homogenized bulk sediment with lithium tetraborate at a 1:20 dilution factor were fused at 1150°C in an induction oven Perle'X-2 to 30-mm-diameter glass discs. The content of major elements Si, Ti, Al, K, Ca, Fe, Mn, Mg, P and Na was calculated as oxide percentages. Analytical accuracy was checked by measuring international standards (GSS-1 to GSS-7) being better than 1% of certified values. Precision of individual measurements was better than 0.9% as determined from replicate analyses of sediment samples (repeatability). Precision over the period of measurement was better than 3.4% (reproducibility) for all elements analyzed in this work. Spurious correlations between elements due to closure effect to 100% are avoided by discussion of element/Al ratios [*Rollinson*, 1993].

[17] X-ray diffraction (XRD) analyses were carried out in selected samples using a Siemens D-500 X-ray diffractometer on untreated, glycolated and heated (550°C) samples. Prior to the analysis, samples were mounted on smear slides after clay separation by decantation.

4. Chronostratigraphy

[18] *Sierro et al.* [2005] provided an age model for core MD99-2343 based on four ^{14}C AMS dates and several tie points with the Greenland ice core GISP2. This age model has been modified to account for six additional monospecific foraminifer ^{14}C AMS dates of which four lie within the 0–12 ka interval (Table 1). A mid Termination Ib (TIb) additional tie point has been added by correlating the Minorca *G. bulloides* oxygen isotopic record to the one from the Alboran Sea core MD95-2043 [*Cacho et al.*, 1999] (Table 1). Both oxygen isotopic profiles for the last 12 kyr are plotted in Figure 3.

[19] Sedimentation rates for the upper 4 m of core MD99-2343 range between 18 and 73 cm kyr^{-1} with an average value of 37 cm kyr^{-1} (Figure 3). These rates are much higher than those determined for nearby sites (e.g., 4 cm kyr^{-1} in core SL87 south of Minorca [*Weldeab et al.*, 2003]), even accounting for potential core stretching [*Skinner and McCave*, 2003]. The high rates likely reflect local enhancement of particle deposition associated with the building of the Minorca sediment drift, as illustrated by seismic

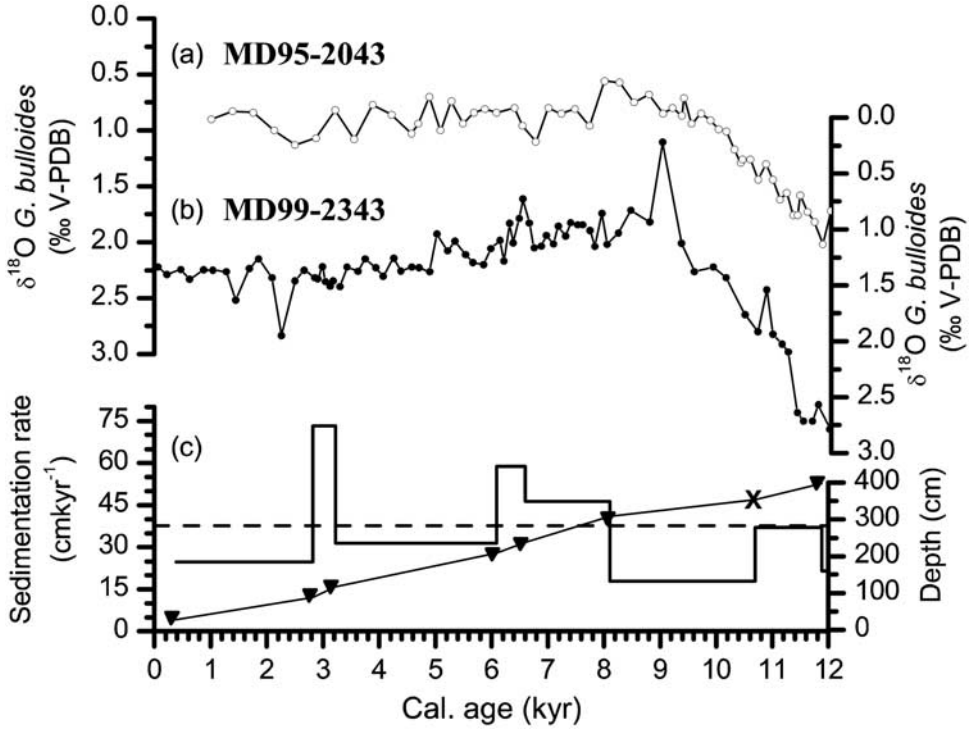

Figure 3. Comparison of the *G. bulloides* oxygen isotopic records from (a) MD95-2043 (Alboran Sea) and (b) MD99-2343 (this study) cores for the last 12 kyr. (c) Sedimentation rates along MD99-2343 sediment core calculated linearly among calendar years from ^{14}C accelerator mass spectrometry (AMS) dates (triangles) and tie points (cross) utilized in the age model (see text for details and Table 1). The mean sedimentation rate of 37 cm kyr^{-1} is represented by a dashed line.

reflection profiles (Figure 2b). Because of the variation in sedimentation rates as a consequence of the sedimentary environment and because of the number of available dates, the final age model was constructed by linear interpolation between calibrated ages instead of using other age-depth extrapolation models [*Telford et al.*, 2004]. The age model accuracy and the sampling interval result in a mean time resolution of 135 years for the top 4 m section of core MD99-2343.

5. Results

5.1. Oxygen Isotopic Record

[20] The heaviest values in the *G. bulloides* δ^{18}O record from core MD99-2343 during the last 12 kyr correspond to the late Younger Dryas (12–11.5 ka) (Figure 4). During the deglaciation (11.5–9 ka), the δ^{18}O record shows a continuously decreasing trend that ends at 9 ka when the lightest δ^{18}O values were reached. The Holocene is characterized by a long-term rising trend punctuated by nine centennial to millennial-scale oscillations (Figure 4a). Some of the δ^{18}O increases are significant, e.g., >0.5‰ from 6.5 to 5.8 ka, or >0.9‰ from 9 to 7.8 ka. Moreover, as discussed below, these oxygen isotopic anomalies (arrows in Figures 4, 5, and 6 and Table 2) correlated with changes in other proxies (see below). We name these events as "Minorca abrupt events" with M8 being the oldest and M0 the youngest. M0 is not very well expressed in the δ^{18}O record but we have also labeled this event considering the other studied proxies. The duration and intensity of these δ^{18}O shifts are similar to those recorded during some of the glacial period Dansgaard/Oeschger cycles [*Sierro et al.*, 2005] and only M0 may fit within the δ^{18}O analytical error. Following previous results [*Cacho et al.*, 1999; *Shackleton et al.*, 2000; *Skinner and Shackleton*, 2003; *Sierro et al.*, 2005] these δ^{18}O fluctuations would be driven by SST coolings of about 2° to 3°C. However, the influence of other properties (i.e., salinity) on the isotopic signal cannot be discarded with the available information.

5.2. Grain Size Distribution

[21] Down-core trends in median grain size are similar for bulk sediment and the noncarbonate fraction (Figures 4b and 4c). The median grain size ranges between 5 and 8 μm, thus pointing to the same processes controlling the deposition of the two fractions. Only a small number of samples from the noncarbonate fraction have median grain sizes coarser than 10 μm. Since the carbonate fraction integrates biological production plus detrital carbonate particles, it is considered that the fraction better representing the intensity of bottom currents is the noncarbonate one [*McCave et al.*, 1995]. This noncarbonate fraction displays seven median grain size peaks at 8.4, 7.2, 6.2, 5, 4.1, 3.2 and 2.5 ka, which are coincident with isotopic enrichment events, i.e., M8 to M2 (Figures 4a and 4c).

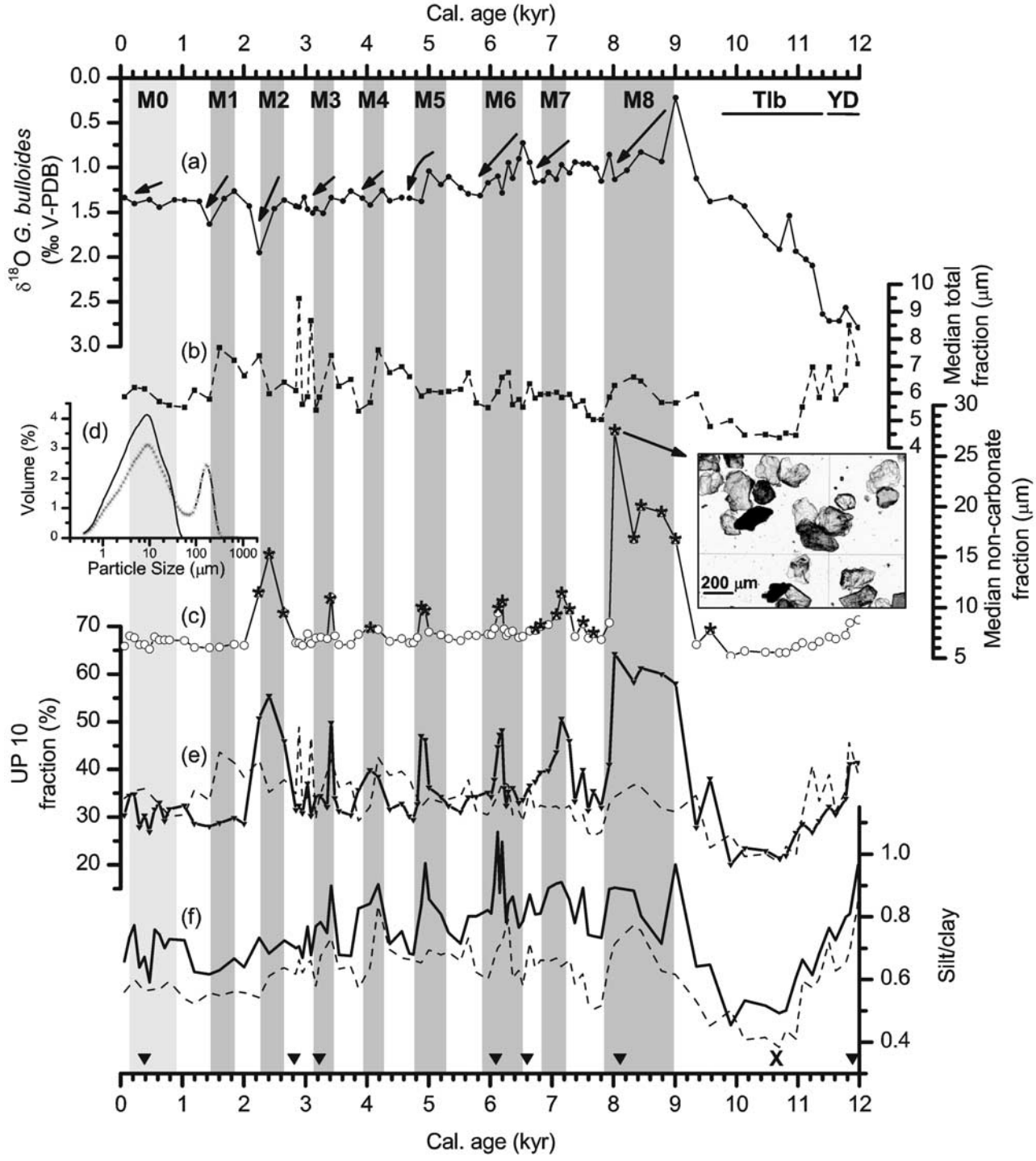

Figure 4. (a) *G. bulloides* oxygen isotopic record from core MD99-2343 for the last 12 kyr. Grain size records of the (b) total and (c) noncarbonate fraction of the sediment, expressed as the median (μm) of each sample. The image is a plane light photograph of the noncarbonate fraction coarser than 63 μm from 304-cm core depth. Asterisks indicate bimodal samples. (d) Examples of unimodal (solid line, sample between M5 and M6) and bimodal (dotted line, from one M7 sample) grain size distributions. (e) UP10 fraction (>10 μm) and (f) silt/clay ratio for the noncarbonate fraction (solid line) and the total fraction (dashed line). Arrows and bars indicate the position of the Minorca abrupt events M8 to M0 as defined in the text. The ^{14}C AMS dates (triangles) and tie point (cross) are also shown.

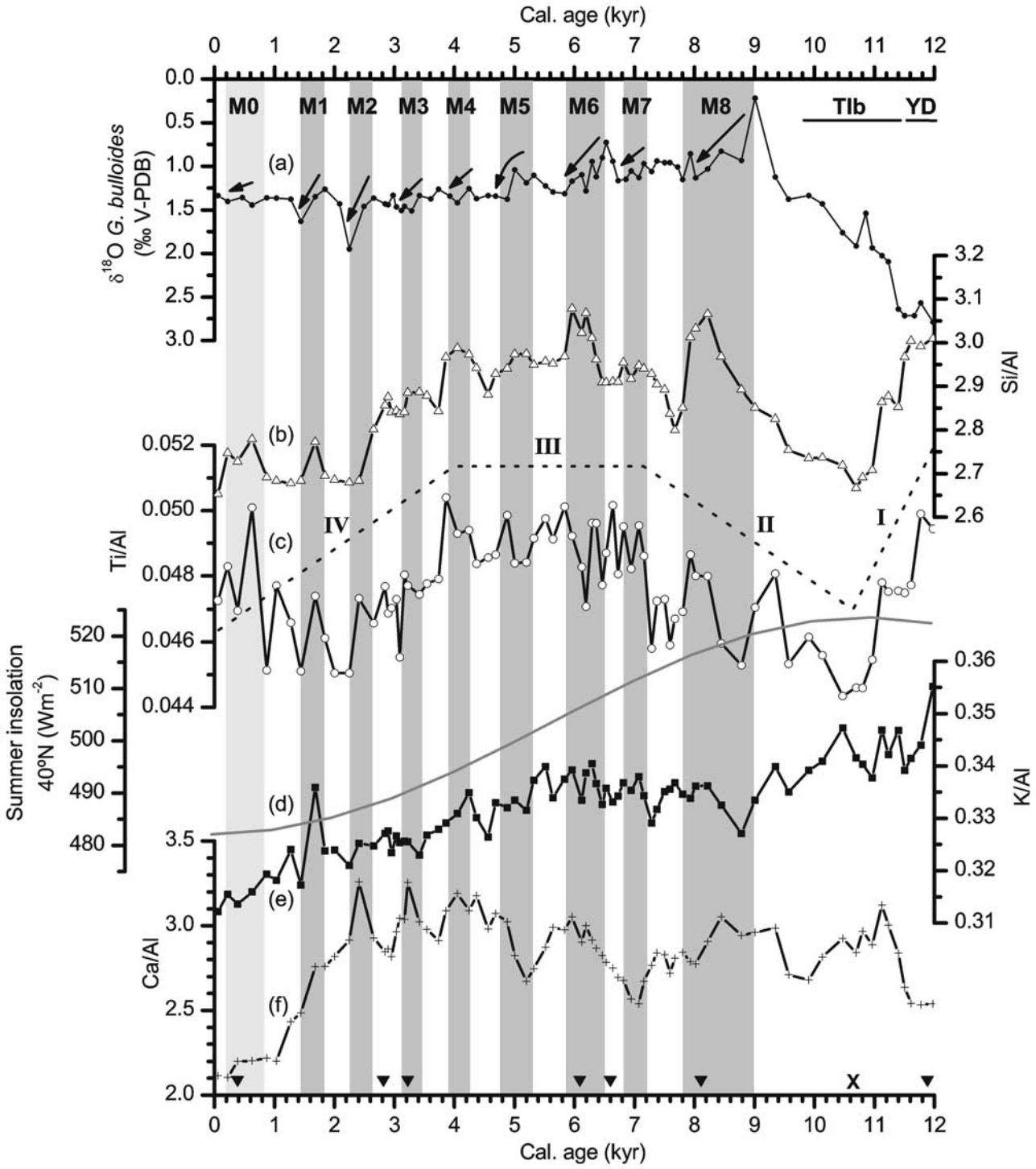

Figure 5. (a) *G. bulloides* oxygen isotopic record from core MD99-2343 for the last 12 kyr. (b) Si, (c) Ti, (e) K, and (f) Ca geochemical records from core MD99-2343 normalized to Al. (d) Summer insolation curve at 40°N for the last 12 kyr. A dashed line between Si/Al and Ti/Al ratios represents the four distinct phases described in the general trend (see text). Arrows and grey bars indicate the Minorca abrupt events M8 to M0 as defined in the text. The ^{14}C AMS dates (inverted triangles) and tie point (cross) are also shown.

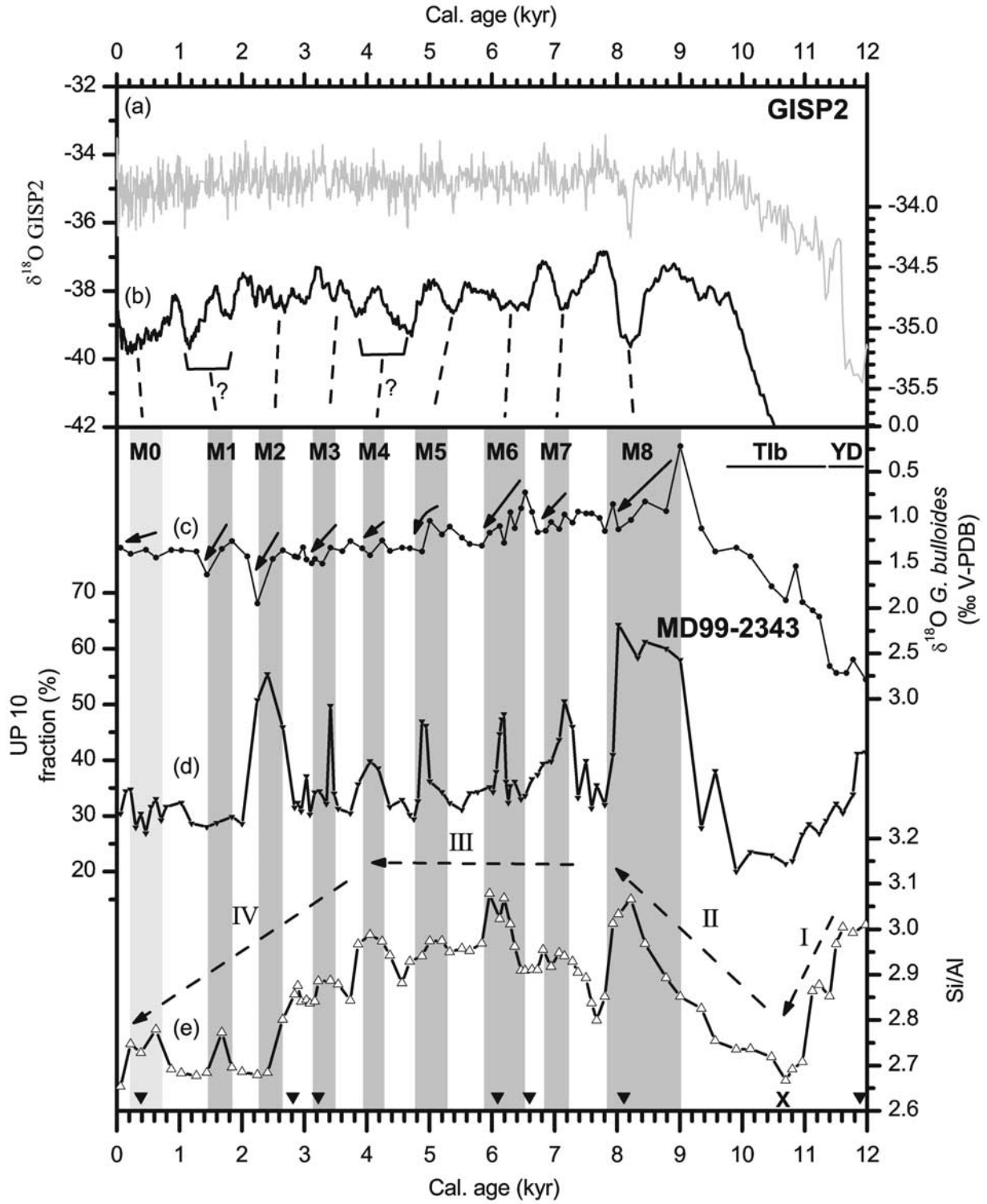

Figure 6. (a) Continuous and (b) 300-year running mean records of the oxygen isotopic profile from the GISP2 ice core [*Grootes et al.*, 1993; *Meese et al.*, 1997]. (c) *G. bulloides* oxygen isotopic record from core MD99-2343 for the last 12 kyr. (d) UP10 fraction (>10 μm) record for the noncarbonate fraction. (e) Si/Al profile with an indication of the four phases identified (I–IV). The arrows and the grey bars represent the nine Minorca abrupt events M8 to M0. Dashed lines represent an attempt to correlate the Minorca events with the oxygen isotopic record from the GISP2 ice core. The ^{14}C AMS dates (inverted triangles) and tie point (cross) are also shown.

Table 2. Timing of Holocene Abrupt Climate Events[a]

Event	Central Age, ka	Time Since Previous Event, ka	Age Interval, ka	Duration, ka	Cold Events in the North Atlantic and Mediterranean Regions				Global Compilation of Events
					SST Alboran	Lakes and Rivers Mediterranean	IRD North Atlantic	Salt and Dust Greenland	
M0	0.5	1.1	0.8–0.2	0.6	-	0.8	-	0.6–0	0.6–0.15
M1	1.6	0.9	1.8–1.4	0.4	1.4	2	1.4	-	1.2–1
M2	2.5	0.7	2.6–2.3	0.3	-	-	-	3.1–2.4	–
M3	3.2	0.9	3.4–3.1	0.3	-	3	2.8		3.5–2.5
M4	4.1	0.9	4.2–4	0.2	-	4	4.2	-	4.2–3.8
M5	5	1.2	5.3–4.7	0.6	5.4	-	-	6.1–5	6–5
M6	6.2	0.9	6.5–5.8	0.7	-	-	5.9	-	-
M7	7.2	1.5	7.4–6.9	0.5	-	7	-	-	-
M8	8.4	-	9–7.8	1.2	8.24	9	8.1	8.8–7.8	9–8

[a]Timings of the Holocene Minorca abrupt events found in core MD99-2343 and tentative correlation with abrupt events recorded from SST in the Alboran Sea [*Cacho et al.*, 2001], in lakes and rivers from the Mediterranean region [*Magny et al.*, 2002], in ice-rafted detritus (IRD) from the North Atlantic region [*Bond et al.*, 1997], in salt and dust from Greenland ice [*O'Brien et al.*, 1995], and the compilation of Holocene rapid climate change events from *Mayewski et al.* [2004].

[22] A detailed study of grain size distributions from the noncarbonate fraction reveals that most of the samples within the Holocene are unimodal, with mode values around 8–10 μm (Figure 4d). Few samples show bimodal distributions with a second mode around 150–200 μm (Figure 4d), which is given by the presence of coarser grains, mainly quartz and mica packets, as observed by microscope (see photograph in Figure 4c). Such bimodal samples (marked with an asterisk in Figure 4c) correspond, with rare exceptions, to the samples with high median grain size values in the noncarbonate fraction and hence to the Minorca abrupt events M8 to M2.

[23] The UP10 general trend mimics the median grain size records and highlights additional features (Figures 4b, 4c, and 4e), for example a marked decrease from 11.5 to 10 ka, and a better expression of M4 (Figure 4a). From 9 ka to present, the UP10 fraction oscillates between 30 and 35%, except for M8 to M2 events. In the M8 to M2 peaks the UP10 fraction may represent as much as 50% of the sample (Figure 4e). The UP10 peaks are consistent with the above mentioned median grain size increases (Figure 4c), and correlative with the oxygen isotopic enrichments of the Minorca abrupt events (Figure 4a). A slight increase in the UP10 fraction is recognized in the last millennium.

[24] Silt/clay ratio (Figure 4f) complements the information gathered from grain size parameters. Like UP10, this ratio also illustrates a marked fall of silt accumulation during the deglaciation, displays relatively high values during the early Holocene and shows a decreasing trend during the last 9 kyr ending with relatively low values during the late Holocene (Figure 4f). The overall record is again punctuated by a number of peaks linked to the Minorca abrupt events identified from previous proxies. These long-term trends and short-lived events are visible in both the bulk (dashed lines in Figure 4) and the noncarbonate fraction (solid lines in Figure 4), where they are more obvious.

5.3. Geochemical Record

[25] The Si/Al, Ti/Al, K/Al and Ca/Al geochemical profiles of core MD99-2343 are plotted in Figures 5b, 5c, 5e, and 5f. Four main phases or trends are identified through the last 12 kyr: I, a decreasing trend in Si/Al and Ti/Al ratios (Figures 5b and 5c) during the deglaciation that leads to a minimum at 10.5 ka that coincides with minimum values in grain size proxies (Figure 4) and maximum values of summer solar insolation at 40°N (Figure 5d); II, an increasing trend in both Si/Al and Ti/Al ratios coincides with the end of the second phase of Termination (TIb) and the early Holocene (10.5–7 ka); III, high Si/Al and Ti/Al ratios with moderate oscillations during the mid-Holocene (7–4 ka); and IV, a gradual decreasing trend in Si/Al and Ti/Al during the late Holocene (4–0 ka), which parallels the decrease in the insolation curve (Figure 5d). Interestingly, the K/Al record (Figure 5e) presents a distinctive pattern during TIb and the early Holocene (phases I and II), therefore suggesting the operation of differentiated controlling factors on K/Al. The Ca/Al ratio (Figure 5f) shows a rather distinct pattern with an almost continuous increasing trend across the Younger Dryas, TIb and early and mid-Holocene, with maximum values between 4 and 2.4 ka that drop abruptly after 2.4 ka (Figure 5f).

[26] The above described general trends are punctuated by oscillations lasting from centuries to millennia. The Si/Al record shows eight abrupt events during the Holocene that are centered at 8.4, 7.2, 6.2, 5, 4.1, 3.2, 1.6 and 0.5 ka (Figure 5b). Most of these events can be identified in the Ti/Al and Ca/Al records as well (Figures 5c and 5f). However, they are not noticeable in the K/Al record (Figure 5e). The abrupt events in the geochemical records coincide with the Minorca abrupt events identified in the *G. bulloides* oxygen isotopic record and the grain size proxies. The only exception to the described overall pattern is M2, which is represented by one of the largest isotopic excursions (Figure 5a), and a Ca/Al peak but lacks of expression in the Si/Al record (Figures 5f and 5b).

[27] The main mineralogical components obtained from the clay size XRD analysis confirm the high percentage of calcite and illite within all the analyzed samples, with chlorite, kaolinite, quartz and very low percentages of feldspars. The lack of major changes in the mineralogical composition of the clay fraction shows that geochemical variability is dominated by the composition of the coarser fraction. This enhances the value of the geochemical

records for the interpretation of processes controlling coarse particle release, transport and accumulation.

6. Discussion

6.1. Particle Sources

[28] Sediment particles resulting from riverine influx, aeolian transport and sea surface biogenic production (see section 2.2) form a mixed population that is expected to settle in the water column where it is advected by water mass movements before final deposition on the seabed. The proxies used in our study allow identifying the ultimate factors controlling sediment deposition in the MD99-2343 core site.

[29] The location of the core MD99-2343 on a sediment drift off the carbonate shelf of the Balearic Islands points to a mixed signal in our Ca/Al ratio resulting from carbonate productivity [*Rühlemann et al.*, 1999] and resedimented carbonate particles [*Van Os et al.*, 1994]. Surface productivity and subsequent particle settling in such an oligotrophic area [*Bethoux et al.*, 1998] can contribute only partly to the carbonate flux and to the relatively high sedimentation rates of core MD99-2343.

[30] Most of the samples within the Minorca abrupt event layers display a characteristic bimodal distribution (Figures 4c and 4d) that could be tentatively attributed to pulses of enhanced aeolian transport. The relatively low rates of Saharan dust deposition and the high sedimentation rates measured in our core lead us to consider the aeolian contribution as largely diluted within particle populations from other sources. In addition, the coarser grains from these layers yield a 150–200 μm mode that is much coarser than the one found in modern and glacial Saharan dust samples in the western Mediterranean [*Guerzoni et al.*, 1997; *Moreno et al.*, 2002]. Furthermore, microscope inspection of the coarse grains observed within the Minorca event layers shows quartz grains with moderate angularity and undisturbed mica packets (sea photograph in Figure 4c), an uncommon feature in aeolian dust particles [*Guerzoni et al.*, 1997]. Those observations point to a rather proximal source for these coarse grains whose release and transport did not involve particularly aggressive physical or chemical weathering processes as would be the case for the aeolian transported particles.

[31] Core MD99-2343 was recovered from a contourite drift and the occurrence of this coarse grain population may be related to the formation of the drift itself. The building of the contourite drift demonstrates the efficiency of deepwater circulation in the area to rework, winnow, transport and accumulate originally fluvial terrigenous particles from the Valencia Valley and therefore explains the relatively high sedimentation rates observed in core MD99-2343. We interpret changes in the grain size distribution as mostly governed by the strength of such deep currents as previously observed in other contourite systems [*McCave and Tucholke*, 1986; *Llave et al.*, 2006; *Voelker et al.*, 2006]. Intervals of enhanced currents resulted in a more efficient transport of coarse particles from both far fluvial sources and local sources as pointed out by the presence of coarse quartz and mica grains with minimal alteration. A prominent volcanic ridge [*Maillard and Mauffret*, 1999] at the very head of the Minorca peripheral depression (Figure 2a), to the west of the Minorca drift, is a firm candidate as source area for such unaltered particles. Therefore the coarse particles deposited during the Minorca abrupt events accumulated during intervals of near-bottom current strengthening able to vigorously erode seafloor relieves and transport to the sediment drift location the coarse particles thus released.

[32] K/Al, Si/Al and Ti/Al ratios are associated with terrigenous inputs [*Krom et al.*, 1999; *Wehausen and Brumsack*, 1999, 2000; *Moreno et al.*, 2001, 2002; *Martínez-Ruiz et al.*, 2003; *Weldeab et al.*, 2003; *Moreno et al.*, 2005], probably from the Ebro and Rhône rivers north of the study site. Si mostly comes from aluminosilicates and quartz as biogenic opal is a minor sediment component in the region [*Weldeab et al.*, 2003], as further confirmed by our microscopic examinations. Ti resides within heavy minerals such as ilmenite and rutile, and Al and K are associated with clay minerals. In particular, the K/Al ratio is considered a good indicator for clay inputs (mainly illite) from river runoff. The presence of noticeable amounts of illite at the study site has been confirmed by peaks in XRD diffractograms. Consequently, the K/Al ratio can be interpreted as an indicator of illite entrance by river discharge and hence may provide a diagnosis of humidity conditions in the northwestern Mediterranean region. The parallelism between the K/Al record and the insolation curve at 40°N not only for the Holocene (Figures 5d and 5e) but also for the last glacial period (J. Frigola et al., Evidences of abrupt changes in Western Mediterranean Deep Water circulation during the last 50 kyr: A high-resolution marine record from the Balearic Sea, submitted to *Quaternary International*, 2006) reinforce the view that precipitation controls long-term K/Al ratio oscillations. The differences observed between Si/Al and Ti/Al, and the K/Al record (Figures 5b, 5c, and 5e) are attributed to grain size geochemical segregation processes since K is mostly associated with clay particles while Si and Ti relate to coarser grains. Parallel increases of the median grain size and the Si/Al and Ti/Al ratios support the view that grain size distribution controls the variability of these geochemical ratios rather than changes in source area.

6.2. Holocene Onset and General Trends

[33] The decrease in the oxygen isotopic record from 12 to 9 ka (Figure 4a) embraces the end of the Younger Dryas, the second phase of Termination (TIb), and the onset of the Holocene. The variations observed in both grain size and geochemical records during this time interval (Figures 4 and 5) reflect the strong changes in the sedimentary dynamics driven by the shifting climatic conditions. Diminutions in grain size parameters and Si/Al and Ti/Al ratios (phase I), which reached minimum values between 10 and 11 ka (Figures 4 and 5), are consistent with a slowdown of deepwater circulation in the western Mediterranean. Accordingly, the glacial benthic isotopic record from our core ends at 12 ka when *C. pachydermus* disappears from the benthic assemblage [*Reguera*, 2004; *Sierro et al.*, 2005], likely replaced by species inhabiting poorly oxygenated environments [*Caralp*, 1988; *Reguera*,

2004]. Reduced deepwater ventilation conditions for this time interval (12–9 ka) are also suggested by the preservation of an Organic Rich Layer in the Alboran Sea [*Cacho et al.*, 2002]. In parallel, TIb sedimentation rates were minimal (Figure 3c) because of the combined effect of the reduction in the input of terrigenous particles forced by the inshore migration of the coastline caused by the postglacial sea level rise, and to a lowered transport of particles into weakened deepwater currents.

[34] The weakening of the deep overturning cell could also result (or be amplified) from more humid conditions in the western Mediterranean region during the time of maximum summer insolation (Figure 5d) as suggested from maximum values of the K/Al record (Figure 5e) and supported by other studies [*Harrison and Digerfeldt*, 1993; *González-Sampériz et al.*, 2006]. A more pronounced stratification in the upper water column favored by an enhanced freshwater input due to increased precipitation during summer insolation maxima, and higher atmospheric stability associated with the retreat of the Northern Hemisphere ice sheet, would have lead to the slowdown of the deepwater overturning cell in the Gulf of Lion and to a reduction of contour current activity in the Minorca sediment drift. After 10.5 ka both grain size and geochemical records show a steady increasing trend (phase II in Figures 5 and 6), which points to the recovery of the deepwater overturning cell in the Gulf of Lion coincident with the decreasing trend in the summer insolation at 40°N (Figure 4d).

[35] The relative stabilization of grain size parameters (Figures 4e and 4f) and the Si/Al ratio around 7 ka (phase III in Figure 6e) is synchronous with the end of the postglacial sea level rise [*Fleming et al.*, 1998] and suggests the reestablishment of deepwater circulation and a stable supply of fluvial material. Such a synchronicity illustrates how significant was the sea level rise control on the western Mediterranean thermohaline circulation and, consequently, on the outbuilding of the Minorca sediment drift. The essentially stable conditions found for the mid-Holocene (7–4 ka) in the Minorca deep sea site contrast with marked changes reported in many locations worldwide [*Steig*, 1999] and, in particular, in the Mediterranean borderlands [*COHMAP Members*, 1988; *Cheddadi et al.*, 1997; *Prentice et al.*, 1998; *Magny et al.*, 2002] and the North African region [*Vernet and Faure*, 2000] associated with the end of the African Humid Period [*deMenocal et al.*, 2000]. This mid-Holocene climate variability is attributed to the reduction of seasonal insolation differences after 5.5 ka, which lead to an abrupt transition from humid to arid conditions in North Africa and in the western Mediterranean region.

[36] This well-known mid-Holocene variability does not seem to influence our proxies until 4 ka when an evident decrease in the silt/clay ratio and the Si/Al points to a slowdown of the deepwater overturning cell and to a reduction of fluvial inputs due to drier conditions (Figure 4f and phase IV in Figure 6e). These drier conditions would be also consistent with the δ^{18}O stabilization at high values during the late Holocene. A southward displacement of the ITCZ and the subsequent decrease in the atmospheric pressure gradient due to reduced seasonal insolation differences likely favored the establishment of drier conditions [*McDermott et al.*, 1999; *Jalut et al.*, 2000]. Accordingly, the lessening in the activity of the northwesterlies would account for the reduction of deepwater circulation during the late Holocene. Our results stress the high sensitivity of the western Mediterranean thermohaline circulation to both the atmospheric (i.e., northwesterlies variability that induced changes in the deepwater overturning in the Gulf of Lion) and the hydrologic systems (i.e., orbitally induced precipitation variability and meltwater pulses).

6.3. Holocene Abrupt Events

[37] The nine Holocene δ^{18}O enrichment events had an average duration of 500 years and an observed periodicity close to 1000 years (Table 2 and Figure 6). Most of the Holocene increases in the oxygen isotopic record parallel increases in the UP10 fraction and the Si/Al ratio (Figure 6), therefore suggesting that relatively cold surface conditions coexisted with more energetic deepwater conditions. An intensification of the northwesterly winds in the western Mediterranean would account for the conditions described during the Holocene Minorca events, similarly to the mechanism proposed for the glacial Dansgaard-Oeschger variability [*Cacho et al.*, 2000; *Sierro et al.*, 2005]. These cold and dry winds enhanced the deepwater overturning in the Gulf of Lion by cooling of the surface waters and, consequently, they steered the activity of bottom currents on the Minorca rise. Such vigorous currents were able to transport coarser particles to the Minorca rise as shown by the accumulation of quartz grains and mica packets coarser than 63 μm. This resulted in the increase of the UP10 fraction (Figure 6d) and the apparition of bimodal samples (Figure 4c). In parallel, higher values in the silt/clay ratio are interpreted as resulting from the winnowing effect of the finest particles (Figure 4f).

[38] While events M8 to M3 are consistently represented in both grain size and geochemical proxies, M0, M1 and M2 are not always well represented. For instance, M2 is not recorded by the Si/Al ratio while it forms one of the larger peaks in the UP10 fraction and, in contrast, M1 and M0 do not show a clear expression in the UP10 ratio but they present significant increases in the Si/Al record (Figure 6). Interestingly, this distinctive sensitivity between the different proxies occurs during the phase IV, late Holocene, related to the establishment of drier conditions due to reduced seasonal insolation differences (section 6.2). Overall, reduced deep overturning is interpreted to occur because of the weakening of northwesterlies and more stable conditions. Furthermore, the expression of the Minorca events in the studied proxies seems to become weaker through the Holocene in parallel to the relative stabilization of the oxygen isotopic signal. These different climatic boundary conditions may have determined a lower sensitivity of the system to millennial-centennial-scale climatic variability toward late Holocene and, consequently, provided an ambiguous signature in the studied records.

[39] The fact that Holocene cooling events have been reported elsewhere all around the globe [*Mayewski et al.*, 2004] demonstrates their global extent and the lack of stability of the Holocene climate. There are, however, disagreements about the precise timing, the character and

the impact of these Holocene abrupt events. Some of the cooling events recorded in the Atlantic and Mediterranean regions are summarized and tentatively correlated to our Minorca cold events M0 to M8 for the last 9 kyr (Table 2). Furthermore, a correlation attempt between the Minorca events and the 300-year running mean of the GISP2 isotopic curve (Figure 6b) results in fairly good agreement, even considering the uncertainties of our age model. This supports the hypothesis of a highly efficient climatic coupling between the North Atlantic and the western Mediterranean region during the last 10 kyr.

[40] The UP10 fraction of our core MD99-2343 displays a periodic oscillation close to 900 years in between 9 and 2 ka (Figure 6e and Table 2), which is in agreement with those obtained from the GISP2 ice core oxygen isotopic record [*Schulz and Paul*, 2002], from a Saharan dust record [*Kuhlmann et al.*, 2004], and from varved sediments in California [*Nederbragt and Thurow*, 2005]. Several hypotheses aim at explaining the periodicity of about 900 years. Though it may be triggered by insolation changes or result from internal feed back mechanisms [*Schulz and Paul*, 2002], the recorded climatic oscillations are better linked to the temperature signal from the North Atlantic climate system, in agreement with other records from the Northern Hemisphere [*Cacho et al.*, 2001; *Kuhlmann et al.*, 2004].

[41] The most pronounced Holocene abrupt event, M8, occurred at 9–7.8 ka, therefore embracing the well-known 8.2 ka cold North Atlantic event [*Mayewski et al.*, 2004; *Alley and Agustsdottir*, 2005; *Rohling and Pälike*, 2005]. The intensification of the atmospheric circulation during M8 led to good ventilation conditions in the Western Mediterranean Basin thus stopping the formation of the ORL in the Alboran Sea [*Cacho et al.*, 2002], synchronously with the middle interruption of sapropel S1 in the Eastern Mediterranean Basin [*Rohling et al.*, 1997; *Mercone et al.*, 2000]. We propose that the atmospheric teleconnection between high latitudes and the Mediterranean region through the westerly winds system was the main control over the western Mediterranean thermohaline circulation through the Holocene. This atmospheric forcing of the climate variability for the last 10 kyr is quite similar to the present pattern of the North Atlantic Oscillation (NAO) that exerts a first-order control at decadal scales [*Rodó et al.*, 1997]. Positive NAO years are associated with Iberian dryness and cold temperatures in Greenland, and more persistent and stronger winter storms crossing the Atlantic Ocean [*Hurrell*, 1995]. Consequently, the Minorca abrupt events could be associated with periods of persistent positive NAO index, which would strengthen the northwesterlies over the northwestern Mediterranean Basin and hence reinforce deepwater overturning. Although we do not exclude a pervasive solar influence or instabilities inherent to the North Atlantic thermohaline circulation [*Bond et al.*, 2001; *Schulz and Paul*, 2002] as main precursors of the Holocene climate oscillations recorded in the core MD99-2343, we suggest that the rapid transmission of these changes from high latitudes to the Mediterranean region was mainly driven by the northwesterly wind system variability modulated by a NAO-like mechanism. A similar atmospheric linkage mechanism, though acting at a millennial scale, was proposed to explain the Dansgaard/Oeschger variability in the deepwater ventilation and Saharan dust input during the last glacial period in the Alboran Sea [*Cacho et al.*, 2000; *Moreno et al.*, 2002; *Sánchez-Goñi et al.*, 2002].

7. Conclusions

[42] The sedimentary record from core MD99-2343 recovered from a deepwater contourite drift reveals the effects of Holocene climate variability over the thermohaline circulation in the Western Mediterranean Basin during the last 12 kyr. Geochemical proxies associated with terrigenous inputs like Si/Al, Ti/Al and K/Al display a decreasing trend through the Holocene that parallels the summer insolation curve at 40°N showing the marked influence of the precipitation pattern over the region. Four different phases have been identified in the Si/Al and Ti/Al ratios from the last 12 kyr. The first from 12 to 10.5 ka shows a slowdown of deepwater circulation due to the combined effect of the increasing sea level and the relatively humid conditions installed on land which both favored the stratification of water masses. The second phase (10.5–7 ka) is associated with the recovery of deepwater circulation until the end of the postglacial sea level rise at 7 ka. The third phase (7–4 ka) corresponds to a plateau with high values of the terrigenous proxies translating the good functioning of deepwater circulation during a progressive orbitally driven change toward dryer conditions in the western Mediterranean borderlands. Finally, the fourth phase (4–0 ka) indicates a progressive decrease of the terrigenous contributions because of reduced fluvial inputs during drier conditions induced by lower seasonal insolation differences, also modulated by the thermohaline circulation weakening because of more stable atmospheric conditions.

[43] Superimposed on this general Holocene pattern, marked oscillations have been noticed and related to abrupt climate changes. The new grain size parameter presented in this work that represents the fraction coarser than 10 μm (UP10) has been tested as a convenient proxy for paleocurrent intensity in the study area for Holocene sediments. The UP10 record presents a 900-year cycle oscillation, which is consistent with the geochemical record of terrigenous input between 9 and 2 ka and the surface cooling events uncovered by the oxygen isotopic record. Such periodicity fits with temperature oscillations from the Holocene δ^{18}O record in Greenland and points to the pressure gradient system as a direct teleconnection mechanism for climate variability transfer from the North Atlantic to the Mediterranean region. The centennial to millennial-scale Holocene oscillations observed in our records reveal a coupled atmospheric/oceanographic forcing equivalent to the present-day NAO and sustains the hypothesis of a rapid fitting with Mediterranean climate conditions. Furthermore, our results demonstrate the high sensitivity of deepwater overturning in the Gulf of Lion to the transfer of climate oscillations from high latitudes to midlatitudes.

[44] **Acknowledgments.** Funding by the European Commission Fifth and Sixth Framework Programmes to projects ADIOS (EVK3-2000-00035), PROMESS 1 (EVR1-CT-2002-40024), EUROSTRATAFORM

(EVK3-2002-00079), and HERMES (GOCE-CT-2005-511234-1) supported the research effort behind this paper. The Spanish-funded BTE2002-04670 and REN2003-08642-C02-02 projects are equally acknowledged. We are especially grateful to the *Marion Dufresne* and the IMAGES programme that enabled the collection of cores MD99-2343 and MD95-2043. GRC Geociències Marines is recognized within the Generalitat de Catalunya excellence research groups program (reference 2005SGR 00152). We thank M. Guart (Departament d'Estratigrafia, Paleontologia i Geociències Marines, University of Barcelona) and E. Seguí (Serveis Cientifico-Tècnics, University of Barcelona) for their help with the laboratory work and G. Lastras and D. Amblas for their help with the artwork. The Editor G. Dickens, J. B. Stuut, and two anonymous reviewers are greatly acknowledged for their positive comments on an earlier version of the manuscript. COMER Foundation and I3P postdoctoral programme (CSIC) are also acknowledged for their support to I. Cacho and A. Moreno, respectively. J. Frigola benefited from a fellowship of the University of Barcelona.

References

Acosta, J. (2005), El Promontorio Balear: Morfología submarina y recubrimiento sedimentario, Ph.D. thesis, 154 pp., Univ. de Barcelona e Inst. Español de Oceanogr., Barcelona.

Alley, R. B., and A. M. Agustsdottir (2005), The 8k event: Cause and consequences of a major Holocene abrupt climate change, *Quat. Sci. Rev.*, *24*, 1123–1149.

Alonso, B., M. Canals, A. Palanques, and J. P. Rehault (1995), A deep-sea channel in the northwestern Mediterranean Sea: Morphology and seismic structure of the Valencia channel and its surroundings, *Mar. Geophys. Res.*, *17*, 469–484.

Barry, R. G., and R. J. Chorley (1998), *Atmosphere, Weather and Climate*, 7th ed., 409 pp., Routledge, London.

Bethoux, J. P., P. Morin, C. Chaumery, O. Connan, B. Gentili, and D. Ruiz-Pino (1998), Nutrients in the Mediterranean Sea, mass balance and statistical analysis of concentrations with respect to environmental change, *Mar. Chem.*, *63*, 155–169.

Bianchi, G. G., and I. N. McCave (1999), Holocene periodicity in North Atlantic climate and deep-ocean flow south of Iceland, *Nature*, *397*, 515–517.

Bolle, H.-J. (2003), *Mediterranean Climate: Variability and Trends*, 372 pp., Springer, New York.

Bond, G., W. Showers, M. Cheseby, R. Lotti, P. Almasi, P. de Menocal, P. Priore, H. Cullen, I. Hajdas, and G. Bonani (1997), A pervasive millennial-scale cycle in North Atlantic Holocene and glacial climates, *Science*, *278*, 1257–1266.

Bond, G., B. Kromer, J. Beer, R. Muscheler, M. Evans, W. Showers, S. Hoffmann, R. Lotti-Bond, I. Hajdas, and G. Bonani (2001), Persistent solar influence on North Atlantic climate during the Holocene, *Science*, *294*, 2130–2136.

Cacho, I., J. O. Grimalt, C. Pelejero, M. Canals, F. J. Sierro, J. A. Flores, and N. J. Shackleton (1999), Dansgaard-Oeschger and Heinrich event imprints in Alboran Sea temperatures, *Paleoceanography*, *14*, 698–705.

Cacho, I., J. O. Grimalt, F. J. Sierro, N. J. Shackleton, and M. Canals (2000), Evidence for enhanced Mediterranean thermohaline circulation during rapid climatic coolings, *Earth Planet. Sci. Lett.*, *183*, 417–429.

Cacho, I., J. O. Grimalt, M. Canals, L. Sbaffi, N. Shackleton, J. Schönfeld, and R. Zahn (2001), Variability of the western Mediterranean Sea surface temperature during the last 25,000 years and its connection with the Northern Hemisphere climatic changes, *Paleoceanography*, *16*, 40–52.

Cacho, I., J. O. Grimalt, and M. Canals (2002), Response of the western Mediterranean Sea to rapid climate variability during the last 50,000 years: A molecular biomarker approach, *J. Mar. Syst.*, *33-34*, 253–272.

Canals, M. (1980), Sedimentos y procesos en el margen continental sur-Balear: Control climático y oceanográfico sobre su distribución y evolución durante el Cuaternario superior, M. S. thesis, 210 pp., Inst. "Jaume Almera" (CSIC) y Univ. de Barcelona, Barcelona.

Caralp, M. H. (1988), Late glacial to recent deep-sea benthic foraminifera from the northeastern Atlantic (Cadiz Gulf) and western Mediterranean (Alboran Sea): Paleoceanographic results, *Mar. Micropaleontol.*, *13*, 265–289.

Cheddadi, R., G. Yu, J. Guiot, S. P. Harrison, and I. C. Prentice (1997), The climate of Europe 6000 years ago, *Clim. Dyn.*, *13*, 1–9.

Cheddadi, R., H. F. Lamb, J. Guiot, and S. van der Kaars (1998), Holocene climatic change in Morocco: A quantitative reconstruction from pollen data, *Clim. Dyn.*, *14*, 883–890.

Claussen, M., C. Kubatzki, V. Browkin, and A. Ganopolski (1999), Simulation of an abrupt change in Saharan vegetation in the mid-Holocene, *Geophys. Res. Lett.*, *26*, 2037–2040.

COHMAP Members, (1988), Climatic changes of the last 18,000 years: Observations and model simulations, *Science*, *241*, 1043–1052.

Coplen, T. B. (1996), New guidelines for the reporting of stable hydrogen, carbon, and oxygen isotope ratio data, *Geochim. Cosmochim. Acta*, *60*, 3359–3360.

Davis, B. A. S., S. Brewer, A. C. Stevenson, and J. Guiot (2003), The temperature of Europe during the Holocene reconstructed from pollen data, *Quat. Sci. Rev.*, *22*, 1701–1716.

deMenocal, P., J. Ortiz, T. Guilderson, J. Adkins, M. Sarnthein, L. Baker, and M. Yarusinsky (2000), Abrupt onset and termination of the African Humid Period: Rapid climate responses to gradual insolation forcing, *Quat. Sci. Rev.*, *19*, 347–361.

Fleming, K., P. Johnston, D. Zwartz, Y. Yokoyama, K. Lambeck, and J. Chappell (1998), Refining the eustatic sea-level curve since the Last Glacial Maximum using far- and intermediate-field sites, *Earth Planet. Sci. Lett.*, *163*, 327–342.

González-Sampériz, P., B. L. Valero-Garcés, A. Moreno, G. Jalut, J. M. García-Ruíz, C. Martí-Bono, A. Delgado-Huertas, A. Navas, T. Otto, and J. J. Dedoubat (2006), Climate variability in the Spanish Pyrenees during the last 30,000 yr revealed by the El Portalet sequence, *Quat. Res.*, *66*, 38–52.

Grootes, P., M. Stuiver, J. W. C. White, S. J. Johnsen, and J. Jouzel (1993), Comparison of oxygen isotope records from the GISP2 and GRIP Greenland ice cores, *Nature*, *366*, 552–554.

Guerzoni, S., E. Molinaroli, and R. Chester (1997), Saharan dust inputs to the western Mediterranean Sea: Depositional patterns, geochemistry and sedimentological implications, *Deep Sea Res., Part II*, *44*, 631–654.

Hall, I. R., and I. N. McCave (2000), Palaeocurrent reconstruction, sediment and thorium focussing on the Iberian margin over the last 140 ka, *Earth Planet. Sci. Lett.*, *178*, 151–164.

Harrison, S. P., and G. Digerfeldt (1993), European lakes as palaeohydrological and palaeoclimatic indicators, *Quat. Sci. Rev.*, *12*, 233–248.

Hughen, K., et al. (2004), Marine04 marine radiocarbon age calibration, 26–0 ka BP, *Radiocarbon*, *46*, 1059–1086.

Hurrell, J. W. (1995), Decadal trends in the North Atlantic Oscillation: Regional temperatures and precipitation, *Science*, *269*, 676–679.

Intergovernmental Oceanographic Commission, International Hydrographic Organization, and British Oceanographic Data Centre (2003) *Centenary Edition of the GEBCO Digital Atlas* [CD-ROM], Br. Oceanogr. Data Cent., Liverpool, U.K.

Jalut, G., A. Esteban Amat, L. Bonnet, T. Gauquelin, and M. Fontugne (2000), Holocene climatic changes in the western Mediterranean, from south-east France to south-east Spain, *Palaeogeogr. Palaeoclimatol., Palaeoecol.*, *160*, 255–290.

Konert, M., and J. Vandenberghe (1997), Comparison of laser grain size analysis with pipette and sieve analysis: A solution for the underestimation of the clay fraction, *Sedimentology*, *44*, 523–535.

Krom, M. D., A. Michard, R. A. Cliff, and K. Strohle (1999), Sources of sediment to the Ionian Sea and western Levantine basin of the eastern Mediterranean during S-1 sapropel times, *Mar. Geol.*, *160*, 45–61.

Kuhlmann, H., H. Meggers, T. Freudenthal, and G. Wefer (2004), The transition of the monsoonal and the N Atlantic climate system off NW Africa during the Holocene, *Geophys. Res. Lett.*, *31*, L22204, doi:10.1029/2004GL021267.

Lacombe, H., P. Tchernia, and L. Gamberoni (1985), Variable bottom water in the Western Mediterranean Basin, *Prog. Oceanogr.*, *14*, 319–338.

Llave, E., J. Schonfeld, F. J. Hernandez-Molina, T. Mulder, L. Somoza, V. Diaz del Rio, and I. Sanchez-Almazo (2006), High-resolution stratigraphy of the Mediterranean outflow contourite system in the Gulf of Cadiz during the late Pleistocene: The impact of Heinrich events, *Mar. Geol.*, *227*, 241–262.

Loyë-Pilot, M. D., J. D. Martin, and J. Moreli (1986), Influence of Saharan dust on the rain acidity and atmospheric input to the Mediterranean, *Nature*, *321*, 427–428.

Magny, M., C. Miramont, and O. Sivan (2002), Assessment of the impact of climate and anthropogenic factors on Holocene Mediterranean vegetation in Europe on the basis of palaeohydrological records, *Palaeogeogr. Palaeoclimatol. Palaeoecol.*, *186*, 47–59.

Maillard, A., and A. Mauffret (1999), Crustal structure and riftogenesis of the Valencia

Trough (north-western Mediterranean Sea), *Basin Res.*, *11*, 357–379.
Maldonado, A., and M. Canals (1982), El margen continental sur-balear: Un modelo deposicional reciente sobre un margen de tipo pasivo, *Acta Geol. Hisp.*, *17*, 241–254.
Maldonado, A., and D. J. Stanley (1979), Depositional patterns and late Quaternary evolution of two Mediterranean submarine fans: A comparison, *Mar. Geol.*, *31*, 215–250.
Maldonado, A., H. Got, A. Monaco, S. O'Connell, and L. Mirabile (1985), Valencia Fan (northwestern Mediterranean): Distal deposition fan variant, *Mar. Geol.*, *62*, 295–319.
Martin, J.-M., F. Elbaz-Poulichet, C. Guieu, M.-D. Loyë-Pilot, and G. Han (1989), River versus atmospheric input of material to the Mediterranean Sea: An overview, *Mar. Chem.*, *28*, 159–182.
Martínez-Ruiz, F., A. Paytan, M. Kastner, J. M. Gonzalez-Donoso, D. Linares, S. M. Bernasconi, and F. J. Jimenez-Espejo (2003), A comparative study of the geochemical and mineralogical characteristics of the S1 sapropel in the western and eastern Mediterranean, *Palaeogeogr. Palaeoclimatol. Palaeoecol.*, *190*, 23–37.
Martrat, B., J. O. Grimalt, C. Lopez-Martinez, I. Cacho, F. J. Sierro, J. A. Flores, R. Zahn, M. Canals, J. H. Curtis, and D. A. Hodell (2004), Abrupt temperature changes in the western Mediterranean over the past 250,000 years, *Science*, *306*, 1762–1765.
Mauffret, A., M. Labarbarie, and L. Montadert (1982), Les affleurements de series sedimentaires pre-pliocenes dans le bassin Mediterraneen nord-occidental., *Mar. Geol.*, *45*, 159–175.
Mayewski, P. A., E. E. Rohling, J. C. Stager, W. Karlen, K. A. Maasch, L. D. Meeker, E. A. Meyerson, F. Gasse, S. van Kreveld, and K. Holmgren (2004), Holocene climate variability, *Quat. Res.*, *62*, 243–255.
McCave, I. N., and B. E. Tucholke (1986), Deep current-controlled sedimentation in the western North Atlantic, in *The Geology of North America, Volume M, The Western North Atlantic Region*, edited by P. R. Vogt and B. E. Tucholke, pp. 451–468, Geol. Soc. of Am., Boulder, Colo.
McCave, I. N., R. J. Bryant, H. F. Cook, and C. A. Coughanowr (1986), Evaluation of a laser-diffraction-size analyzer for use with natural sediments, *J. Sediment. Res.*, *56*, 561–564.
McCave, I. N., B. Manighetti, and S. G. Robinson (1995), Sortable silt and fine sediment size/composition slicing: Parameters for paleocurrent speed and paleoceanography, *Paleoceanography*, *10*, 593–610.
McDermott, F., S. Frisia, Y. Huang, A. Longinelli, B. Spiro, T. H. E. Heaton, C. J. Hawkesworth, A. Borsato, E. Keppens, and I. J. Fairchild (1999), Holocene climate variability in Europe: Evidence from δ^{18}O, textural and extension-rate variations in three speleothems, *Quat. Sci. Rev.*, *18*, 1021–1038.
Medoc, G. (1970), Observation of formation of Deep Water in the Mediterranean Sea, 1969, *Nature*, *227*, 1037–1040.
Meese, D. A., A. J. Gow, R. B. Alley, P. M. Zielinski, G. A. Grootes, M. Ram, K. C. Taylor, P. A. Mayewski, and J. F. Bolzan (1997), The Greenland Ice Sheet Project 2 depth-age scale: Methods and results, *J. Geophys. Res.*, *102*, 26,411–26,423.
Mercone, D., J. Thomson, and I. W. Croudace (2000), Duration of S1, the most recent sapropel in the eastern Mediterranean Sea, as indicated by accelerator mass spectrometry radiocarbon and geochemical evidence, *Paleoceanography*, *15*, 336–347.
Millot, C. (1999), Circulation in the western Mediterranean Sea, *J. Mar. Syst.*, *20*, 423–442.
Millot, C., and A. Monaco (1984), Deep strong currents and sediment transport in the northwestern Mediterranean Sea, *Geo Mar. Lett.*, *4*, 13–17.
Moreno, A., J. Targarona, J. Henderiks, M. Canals, T. Freudenthal, and H. Meggers (2001), Orbital forcing of dust supply to the North Canary Basin over the last 250 kyrs, *Quat. Sci. Rev.*, *20*, 1327–1339.
Moreno, A., I. Cacho, M. Canals, M. A. Prins, M.-F. Sanchez-Goni, J. O. Grimalt, and G. J. Weltje (2002), Saharan dust transport and high-latitude glacial climatic variability: The Alboran Sea record, *Quat. Res.*, *58*, 318–328.
Moreno, A., I. Cacho, M. Canals, J. O. Grimalt, and A. Sanchez-Vidal (2004), Millennial-scale variability in the productivity signal from the Alboran Sea record, western Mediterranean Sea, *Palaeogeogr. Palaeoclimatol. Palaeoecol.*, *211*, 205–219.
Moreno, A., I. Cacho, M. Canals, J. O. Grimalt, M. F. Sanchez-Goni, N. Shackleton, and F. J. Sierro (2005), Links between marine and atmospheric processes oscillating on a millennial time-scale: A multi-proxy study of the last 50000 yr from the Alboran Sea (western Mediterranean Sea), *Quat. Sci. Rev.*, *24*, 1623–1636.
Nederbragt, A. J., and J. Thurow (2005), Geographic coherence of millennial-scale climate cycles during the Holocene, *Palaeogeogr. Palaeoclimatol. Palaeoecol.*, *221*, 313–324.
O'Brien, S. R., P. A. Mayewski, L. D. Meeker, D. A. Meese, M. S. Twickler, and S. I. Whitlow (1995), Complexity of Holocene climate as reconstructed from a Greenland ice core, *Science*, *270*, 1962–1964.
Oppo, D. W., J. F. McManus, and J. L. Cullen (2003), Deepwater variability in the Holocene epoch, *Nature*, *422*, 277–278.
Paillard, D., L. Labeyrie, and P. Yiou (1996), Macintosh program performs time-series analysis, *Eos Trans. AGU*, *77*(39), 379.
Palanques, A., N. H. Kenyon, B. Alonso, and A. Limonov (1995), Erosional and depositional patterns in the Valencia channel mouth: An example of a modern channel-lobe transition zone, *Mar. Geophys. Res.*, *17*, 503–517.
Pinardi, N., and E. Masetti (2000), Variability of the large scale general circulation of the Mediterranean Sea from observations and modelling: A review, *Palaeogeogr. Palaeoclimatol. Palaeoecol.*, *158*, 153–173.
Prentice, I. C., S. P. Harrison, D. Jolly, and J. Guiot (1998), The climate and biomes of Europe at 6000 yr BP: Comparison of model simulations and pollen-based reconstructions, *Quat. Sci. Rev.*, *17*, 659–668.
Prospero, J. M. (1996), Saharan dust transport over the North Atlantic Ocean and Mediterranean: An overview, in *The Impact of Desert Dust Across the Mediterranean*, edited by S. Guerzoni, and R. Chester pp. 133–151, Kluwer Acad., Dordrecht, Netherlands.
Reguera, I. (2004), Respuesta del Mediterráneo Occidental a los cambios climáticos bruscos ocurridos durante el último ciclo glacial: Estudio de las asociaciones de foraminíferos, Ph.D. thesis, 231 pp., Univ. de Salamanca, Salamanca, Spain.
Rodó, X., E. Baert, and F. A. Comin (1997), Variations in seasonal rainfall in southern Europe during the present century: Relationships with the North Atlantic Oscillation and the El Niño-Southern Oscillation, *Clim. Dyn.*, *13*, 275–284.
Rohling, E. J., and H. Pälike (2005), Centennial-scale climate cooling with a sudden cold event around 8,200 years ago, *Nature*, *434*, 975–979.
Rohling, E. J., F. J. Jorissen, and H. C. de Stigter (1997), 200 year interruption of Holocene sapropel formation in the Adriatic Sea, *J. Micropaleontol.*, *16*, 97–108.
Rohling, E. J., A. Hayes, D. Rijk, D. Kroon, W. J. Zachariasse, and D. Eisma (1998), Abrupt cold spells in the northwest Mediterranean, *Paleoceanography*, *13*, 316–322.
Rohling, E. J., P. A. Mayewski, R. H. Abu-Zied, J. S. L. Casford, and A. Hayes (2002), Holocene atmosphere-ocean interactions: Records from Greenland and the Aegean Sea, *Clim. Dyn.*, *18*, 587–593.
Rollinson, H. (1993), *Using Geochemical Data: Evaluation, Presentation, Interpretation*, 352 pp., Longman Sci. and Technical, New York.
Rühlemann, C., P. J. Müller, and R. Schneider (1999), Organic carbon and carbonate as paleoproductivity proxies: Examples from high and low productivity areas of the tropical Atlantic, in *Use of Proxies in Paleoceanography: Examples From the South Atlantic*, edited by G. Fischer and G. Wefer pp. 1–31, Springer, New York.
Sánchez-Goñi, M. F., I. Cacho, J. L. Turon, J. Guiot, F. J. Sierro, J.-P. Peypouquet, J. O. Grimalt, and N. J. Shackleton (2002), Synchroneity between marine and terrestrial responses to millennial scale climatic variability during the last glacial period in the Mediterranean region, *Clim. Dyn.*, *19*, 95–105.
Sbaffi, L., F. C. Wezel, G. Curzi, and U. Zoppi (2004), Millennial- to centennial-scale palaeoclimate variations during Termination I and the Holocene in the central Mediterranean Sea, *Global Planet. Change*, *40*, 201–217.
Schulz, M., and A. Paul (2002), Holocene climate variability on centennial-to-millennial time scales: 1. Climate records from the North-Atlantic realm, in *Climate Development and History of the North Atlantic Realm*, edited by G. Wefer et al., pp. 41–54, Springer, New York.
Shackleton, N. J., M. A. Hall, and E. Vincent (2000), Phase relationships between millennial-scale events 64,000–24,000 years ago, *Paleoceanography*, *15*, 565–569.
Sierro, F. J., et al. (2005), Impact of iceberg melting on Mediterranean thermohaline circulation during Heinrich events, *Paleoceanography*, *20*, PA2019, doi:10.1029/2004PA001051.
Skinner, L. C., and I. N. McCave (2003), Analysis and modelling of gravity- and piston coring based on soil mechanics, *Mar. Geol.*, *199*, 181–204.
Skinner, L. C., and N. Shackleton (2003), Millennial-scale variability of deep-water temperature and $\delta^{18}O_{dw}$ indicating deep-water source variations in the northeast Atlantic, 0–34 cal. ka BP, *Geochem. Geophys. Geosyst.*, *4*(12), 1098, doi:10.1029/2003GC000585.
Steig, E. J. (1999), Mid-Holocene climate change, *Science*, *286*, 1485–1487.
Stow, D. A. V. (1982), Bottom currents and contourites in the North Atlantic, *Bull. Inst. Geol. Bassin Aquitaine*, *31*, 151–166.
Stow, D. A. V., J. C. Faugères, J. A. Howe, C. J. Pudsey, and A. R. Viana (2002), Bottom cur-

rents, contourites and deep-sea sediment drifts: Current state-of-the-art, in *Deep-Water Contourite Systems: Modern Drifts and Ancient Series, Seismic and Sedimentary Characteristics*, *Geol. Soc. Mem.*, vol. 22, edited by D. A. V. Stow et al., pp. 7–20, Geol. Soc., London.

Stuiver, M., and P. J. Reimer (1993), Extended ^{14}C database and revised CALIB radiocarbon calibration program, *Radiocarbon*, *35*, 215–230.

Telford, R. J., E. Heegaard, and H. J. B. Birks (2004), All age-depth models are wrong: But how badly?, *Quat. Sci. Rev.*, *23*, 1–5.

United Nations Environment Programme (2003) Riverine transport of water, sediments and pollutants to the Mediterranean Sea, *MAP Tech. Rep. Ser. 141*, Athens.

Vanney, R., and D. Mougenot (1981), La plate-forme continentale du Portugal et des provinces adjancetes: Analyse géomorphologique, *Mem. Serv. Geol. Port.*, *28*, 1–86.

Van Os, B. J. H., L. J. Lourens, F. J. Hilgen, G. J. de Lange, and L. Beaufort (1994), The formation of Pliocene and carbonate cycles in the Mediterranean: Diagenesis, dilution and productivity, *Paleoceanography*, *9*, 601–617.

Velasco, J. P. B., J. Baraza, and M. Canals (1996), La depresión periférica y el lomo contourítico de Menorca: Evidencias de la actividad de corrientes de fondo al N del Talud Balear, *Geogaceta*, *20*, 359–362.

Vernet, R., and H. Faure (2000), Isotopic chronology of the Sahara and the Sahel during the late Pleistocene and the early and mid-Holocene (15,000–6,000 BP), *Quat. Int.*, *68–71*, 385–387.

Voelker, A. H. L., S. M. Lebreiro, J. Schonfeld, I. Cacho, H. Erlenkeuser, and F. Abrantes (2006), Mediterranean outflow strengthening during Northern Hemisphere coolings: A salt source for the glacial Atlantic?, *Earth Planet. Sci. Lett.*, *245*, 39–55.

Wehausen, R., and H.-J. Brumsack (1999), Cyclic variations in the chemical composition of eastern Mediterranean Pliocene sediments: A key for understanding sapropel formation, *Mar. Geol.*, *153*, 161–176.

Wehausen, R., and H.-J. Brumsack (2000), Chemical cycles in Pliocene sapropel-bearing and sapropel-barren eastern Mediterranean sediments, *Palaeogeogr. Palaeoclimatol. Palaeoecol.*, *158*, 325–352.

Weldeab, S., W. Siebel, R. Wehausen, K.-C. Emeis, G. Schmiedl, and C. Hemleben (2003), Late Pleistocene sedimentation in the western Mediterranean Sea: Implications for productivity changes and climatic conditions in the catchment areas, *Palaeogeogr. Palaeoclimatol. Palaeoecol.*, *190*, 121–137.

Weltje, G. J., and M. Prins (2003), Muddled or mixed? Inferring palaeoclimate from size distributions of deep-sea clastics, *Sediment. Geol.*, *162*, 39–62.

Zuo, Z., D. Eisma, and G. W. Berger (1991), Determination of sediment accumulation and mixing rates in the Gulf of Lions, Mediterranean Sea, *Oceanol. Acta*, *14*, 253–262.

I. Cacho, M. Canals, and J. Frigola, Consolidated Research Group Marine Geosciences, Department of Stratigraphy, Paleontology and Marine Geosciences, Faculty of Geology, University of Barcelona, Campus de Pedralbes, C/Martí i Franquès s/n, E-08028 Barcelona, Spain. (miquelcanals@ub.edu)

J. H. Curtis and D. A. Hodell, Department of Geological Sciences, University of Florida, Gainesville, FL 32611-2120, USA.

J. A. Flores and F. J. Sierro, Department of Geology, University of Salamanca, Plaza de la Merced s/n, E-37008 Salamanca, Spain.

J. O. Grimalt, Department of Environmental Chemistry, ICER-CSIC, Jordi Girona 18, E-08034 Barcelona, Spain.

A. Moreno, Pyrenean Institute of Ecology, Spanish Research Scientific Council, Aptdo. 202, E-50080 Zaragoza, Spain.